a dimming. This increase has been found to be significant at the 99% level of confidence. The satellite-based record of surface solar fluxes from 1983 until 1992 does suggest some dimming, followed by an increase after 1992, as seen in numerous ground observations. It was also shown that tendencies over land and over ocean can differ in sign and magnitude, and that in order to obtain a global view of the dimming phenomena, there is a need for comprehensive and global observations that are possible only from satellites. There is a need to be aware of calibration issues regarding both ground-based and satellite data that might affect the interpretation of long-term observations. The best available approach to calibration was used to produce the satellite observations used in this study, and the most comprehensive global coverage achievable by combining geostationary and polar-orbiting satellites was used. The magnitudes of the observed tendencies in S at a global scale were much smaller in magnitude than those reported from ground observations.

References and Notes

1. G. Stanhill, S. Cohen, *Agric. For. Meteorol.* **107**, 255 (2001).
2. B. G. Liepert, *Geophys. Res. Lett.* **29**, 10.1029/2002GL014910 (2002).
3. M. Wild *et al.*, in preparation.
4. A. Ohmura, H. Lang, *IRS '88: Current Problems in Atmospheric Radiation*, J. Lenoble, J.-F. Geleyn, Eds. (Deepak Publishing, Hampton, VA, 1989).
5. V. Russak, *Tellus* **42B**, 206 (1990).
6. M. L. Roderick, G. D. Farquhar, *Science* **298**, 1410 (2002).
7. M. Wild, A. Ohmura, H. Gilgen, *Geophys. Res. Lett.* **31**, L11201 (2004).
8. R. Philipona, B. Durr, *Geophys. Res. Lett.* **31**, L22208 (2004).
9. R. Philipona, *Geophys. Res. Lett.* **31**, L03202 (2004).
10. V. Ramanathan, P. J. Crutzen, J. T. Kiehl, D. Rosenfeld, *Science* **294**, 2119 (2001).
11. H. C. Power, *Theor. Appl. Climatol.* **76**, 47 (2003).
12. E. Raveh *et al.*, *J. Exp. Bot.* **54**, 365 (2003).
13. M. L. Roderick, G. D. Farquhar, S. L. Berry, I. R. Noble, *Ecologia* **129**, 21 (2001).
14. W. B. Rossow, R. A. Schiffer, *Bull. Am. Meteorol. Soc.* **72**, 2 (1991).
15. W. B. Rossow, R. A. Schiffer, *Bull. Am. Meteorol. Soc.* **80**, 2261 (1999).
16. C. L. Brest, W. B. Rossow, M. D. Roiter, *J. Atmos. Oceanic Technol.* **14**, 1091 (1997).
17. Y. Desormeaux, W. B. Rossow, C. L. Brest, G. G. Campbell, *J. Atmos. Oceanic Technol.* **10**, 304 (1993).
18. R. T. Pinker, I. Laszlo, *J. Appl. Meteorol.* **31**, 194 (1992).
19. C. H. Whitlock *et al.*, *Bull. Am. Meteorol. Soc.* **76**, 1 (1995).
20. M. Chiacchio, P. W. Stackhouse Jr., S. K. Gupta, S. J. Cox, J. C. Mikovitz, paper presented at the American Geophysical Union 2004 Spring Meeting, Montreal, Quebec, Canada, 2004.
21. P. W. Stackhouse Jr. *et al.*, *GEWEX News* **14**, 10 (2004).
22. B. B. Hicks *et al.*, *Bull. Am. Meteorol. Soc.* **77**, 2857 (1996).
23. R. T. Pinker *et al.*, *J. Geophys. Res.* **108** (D22), 8844 (2003).
24. W. H. Press, B. P. Flannery, S. A. Teukolsky, W. T. Vetterling, *Numerical Recipes in Fortran 90* (Cambridge Univ. Press, Cambridge, ed. 2, 1992).
25. E. G. Dutton *et al.*, *J. Geophys. Res.* **109**, D03204 (2004).
26. X. Wang, J. R. Key, *Science* **299**, 1725 (2003).
27. B. A. Wielicki *et al.*, *Science* **295**, 841 (2002).
28. B. A. Wielicki *et al.*, *Bull. Am. Meteorol. Soc.* **77**, 853 (1996).
29. B. R. Barkstrom, *Bull. Am. Meteorol. Soc.* **65**, 1170 (1984).
30. T. M. Smith, R. W. Reynolds, *J. Clim.* **17**, 2466 (2004).
31. W. B. Rossow, E. N. Duenas, *Bull. Am. Meteorol. Soc.* **85**, 167172 (2004).
32. R. S. Stone, E. G. Dutton, J. M. Harris, D. Longenecker, *J. Geophys. Res.* **107**, 4089 (2002).
33. C. J. Tucker *et al.*, *Int. J. Biometeorol.* **45**, 184 (2001).
34. R. Tateishi, M. Ebata, *Int. J. Remote Sens.* **25**, 2287 (2004).
35. E. Palle, P. R. Goode, P. Montañés-Rodríguez, S. E. Koonin, *Science* **304**, 1299 (2004).

36. Supported under NASA grants NAG59634 (Earth Observing System/Interdisciplinary Science Investigation) and NNG04GD65G (Office of Earth Science) and benefited by work done under NAG5836 (Earth Science Enterprise/HYDROMET/Large Scale Biosphere-Atmosphere Experiment in Amazonia) to the University of Maryland. We appreciate the monumental effort of W. B. Rossow in preparing the ISCCP data; without such information, this study would not have been possible. The ISCCP D1 data were obtained from the NASA Langley Atmospheric Sciences Data Center.

Supporting Online Material

www.sciencemag.org/cgi/content/full/308/5723/850/DC1

Figs. S1 and S2

23 July 2004; accepted 16 March 2005

10.1126/science.1103159

The Holocene Asian Monsoon: Links to Solar Changes and North Atlantic Climate

Yongjin Wang,[1] Hai Cheng,[1,2]* R. Lawrence Edwards,[2] Yaoqi He,[1] Xinggong Kong,[1] Zhisheng An,[3] Jiangying Wu,[1] Megan J. Kelly,[2] Carolyn A. Dykoski,[2] Xiangdong Li[4]

A 5-year-resolution absolute-dated oxygen isotope record from Dongge Cave, southern China, provides a continuous history of the Asian monsoon over the past 9000 years. Although the record broadly follows summer insolation, it is punctuated by eight weak monsoon events lasting ~1 to 5 centuries. One correlates with the "8200-year" event, another with the collapse of the Chinese Neolithic culture, and most with North Atlantic ice-rafting events. Cross-correlation of the decadal- to centennial-scale monsoon record with the atmospheric carbon-14 record shows that some, but not all, of the monsoon variability at these frequencies results from changes in solar output.

The impacts of decadal- to centennial-scale solar variability on the climate system during the Holocene have been reported from mid to high northern latitudes (*1*–*3*) to low-latitude regimes (*4*–*6*), including the Asian monsoon (AM) (*4*, *5*). To test the degree to which the Holocene AM may be linked to solar variability, a high-resolution, precisely dated, continuous record of the monsoon is needed. Such a record could also be used to test the degree to which changes in the interglacial AM are related to climate change elsewhere. For example, a number of studies have demonstrated close ties between the glacial AM and the climate in the North Atlantic region (*7*–*9*). The degree to which such links extend into interglacial periods is an open question. We have previously reported on a Chinese Holocene record of the AM that addresses some of these issues (*10*). Here, we build on that work with a higher resolution absolute-dated Holocene AM record from Dongge Cave, southern China, which we compare in detail with the atmospheric ^{14}C record (as a proxy for solar output) and climate records from the North Atlantic region (*2*, *11*–*13*).

Stalagmite DA was collected from Dongge Cave (25°17′N, 108°5′E, elevation 680 m) in southern China. Today, the cave site has two distinct seasons: a cool, dry season during the boreal winter when the Siberian high establishes a strong anticyclone on the Tibetan Plateau and a warm, wet season during the summer months when the intertropical convergence zone (ITCZ) shifts northward and monsoonal convective rainfall reaches its maximum. Our previous studies have shown that shifts in the oxygen isotope ratio ($\delta^{18}O$) of the stalagmite from the cave largely reflect changes in $\delta^{18}O$ values of meteoric precipitation at the site, which in turn relate to changes in the amount of precipitation and thus characterize the AM strength (*10*, *14*).

Chronology of the 962.5-mm-long stalagmite DA is established by 45 ^{230}Th dates (table S1), all in stratigraphic order, with a typical age uncertainty of 50 years. Sample DA grew continuously from approximately 9000 years before the present (ky B.P., where the "present" is defined as the year 1950 A.D.) until 2002 (when the stalagmite was collected), with a nearly constant growth rate of ~100 μm per year. A total of 2124 $\delta^{18}O$ measurements were obtained

[1]College of Geography Science, Nanjing Normal University, Nanjing 210097, China. [2]Department of Geology and Geophysics, University of Minnesota, MN 55455, USA. [3]State Key Lab of Loess and Quaternary Geology, Institute of Earth Environment, Chinese Academy of Sciences, Xi'an 71005, China. [4]Department of Civil and Structural Engineering, The Hong Kong Polytechnic University, Hung Hom, Kowloon, Hong Kong.

*To whom correspondence should be addressed. E-mail: cheng021@umn.edu

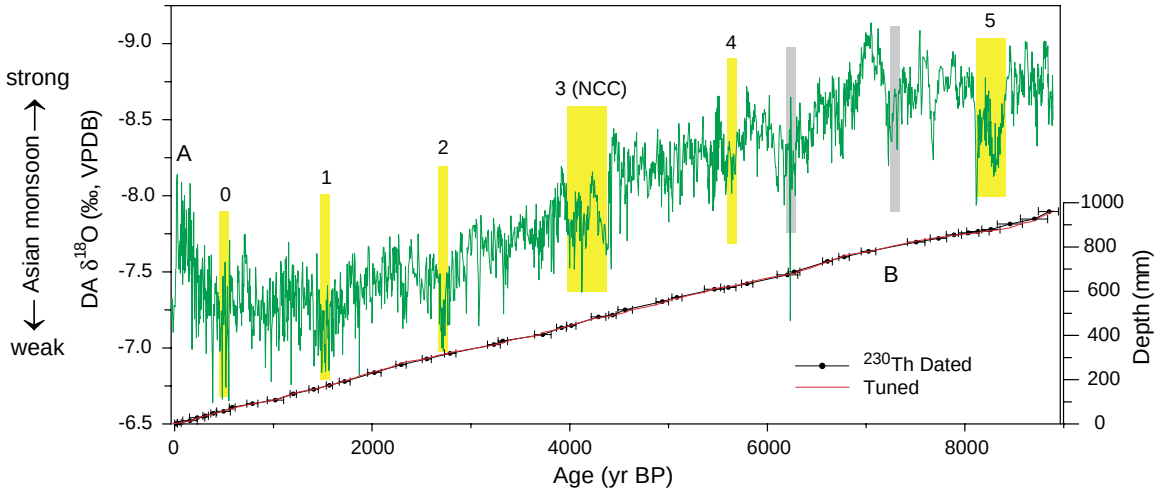

Fig. 1. (**A**) $\delta^{18}O$ time series of the Dongge Cave stalagmite DA (green line). Six vertical yellow bars denote the timing of Bond events 0 to 5 in the North Atlantic (*2*). The Chinese events that correlate with Bond events 3 and 5 coincide within error with the collapse of the Neolithic Culture of China (NCC) (*23*) and the timing of an abrupt outflow event from a Laurentide ice-margin lake (*22*), respectively. Two vertical gray bars indicate two other notable weak AM events that can be correlated to ice-rafted debris events (*2*). (**B**) DA age-depth (mm, relative to the top) relations. Black error bars show ^{230}Th dates with 2σ errors (table S1). We use two different age-depth curves, one employing linear interpolation between dated depths and the second slightly modified by tuning to INTCAL98 (*15*) within the ^{230}Th dating error (*26*).

from along the growth axis, with an average temporal resolution of 4.5 years (table S2). We present two time scales, one of which is based on linear interpolation between the ^{230}Th dates and is independent from all of the chronologies to which we compare our data (Fig. 1). Another is tuned within dating error to INTCAL98 (*15*) (Fig. 1) and is used to determine the extent to which fine-scale dating errors may affect our correlations with other records.

The $\delta^{18}O$ values vary between –9.2 and –6.5 ‰, with a typical amplitude of somewhat less than 1 ‰ over time scales of decades to centuries. As verified by our previous studies (*10*, *14*), Dongge Cave $\delta^{18}O$ becomes lower as Asian summer monsoon intensifies, and vice versa. Such anticorrelation is also observed in the modern precipitation records near the cave site (*16*).

DA $\delta^{18}O$ data shows a strong AM interval from 9 to 7 ky B.P., followed by a gradual weakening. This overall temporal pattern resembles high-resolution Holocene precipitation records from a southern Oman stalagmite (*5*), titanium concentration data from the Cariaco Basin, tropical Atlantic (*17*), and our earlier work (*10*), which suggests that shifts in mean position of the ITCZ may control temporal variability of precipitation throughout the entire low-latitude region (*18*). This general weakening of the Asian monsoon during the Holocene corresponds with orbitally induced lowering of Northern Hemisphere summer solar insolation during this interval, which indicates that the broad trend is caused by insolation change. The general trend is punctuated by eight weak AM events, each lasting ~1 to 5 centuries, centered at 0.5, 1.6, 2.7, 4.4, 5.5, 6.3, 7.2, and 8.3 ky B.P., with a temporal spacing averaging ~1.2 ky (Fig. 1). These events are, within dating error, in phase with weak southwest AM events recorded in marine cores from the Arabian Sea (*19*) and are possibly linked to Holocene ice-rafting events in the North Atlantic (*2*) (Fig. 1). Among those events, the two at 8.4 to 8.1 and 4.5 to 4.0 ky B.P. are longer in duration and larger in magnitude. They are similar in terms of the abrupt transitions and magnitude (0.8 to 1.0 ‰), and they have one or two brief reversions within the events. The event at 8.4 to 8.1 ky B.P. correlates with the strongest Holocene cooling/drying event recorded at high northern latitudes (*1*, *20*) and subtropical temperate regions (*21*) and in tropical ocean and terrestrial records (*4*, *5*, *19*); it also coincides within error with the 8.2-ky event recorded in the Greenland ice cores (*11*, *12*), possibly related to abrupt outflow from a Laurentide ice-margin lake (*22*). Another major event at ~4.4 to 3.9 ky B.P., although not clear in Greenland records, has been reported in various localities in China (*23*). Among the most abrupt events in the Holocene Dongge record is the abrupt lowering of AM intensity at ~4.4 ky B.P. over several decades (Fig. 1 and table S2), which supports the idea that this sharp hydrological change might be responsible for the collapse of the Neolithic culture around Central China about 4.0 ky ago (*23*). Strongly enhanced aridity at this time is also a main feature of the Indian monsoon as recorded in western China (*24*) and is in phase with the Mesopotamian dry event in western Asia (*25*).

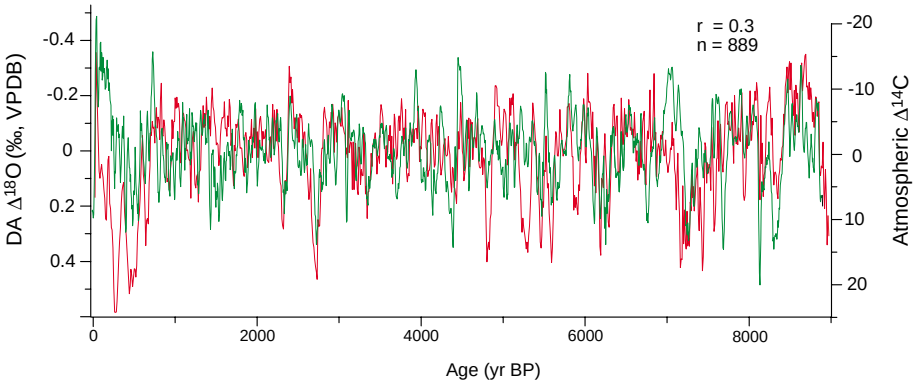

Fig. 2. Time series of the DA $\Delta^{18}O$ record (five-point running average, green line) and the atmospheric $\Delta^{14}C$ record (red line) (*15*). All data have been detrended using singular spectrum analysis. Higher solar irradiance (smaller $\Delta^{14}C$) corresponds to a stronger AM (smaller $\Delta\delta^{18}O$ value). The correlation coefficient is 0.30 for the entire profile and 0.39 between 9 and 6 ky B.P.

To assess the link between solar activity and AM intensity, we compared the detrended DA $\delta^{18}O$ ($\Delta^{18}O$) record to the detrended atmospheric ^{14}C record ($\Delta^{14}C$), a proxy for solar activity (*15*) (Fig. 2), using the tuned time scale for DA (*26*). As the time scale is tuned, we consider the resulting correlation to be a "best case" scenario. Visually, (Fig. 2) the larger amplitude fluctuations in the AM (>±0.2 ‰ in the $\Delta\delta^{18}O$ record) broadly agree with $\Delta^{14}C$ events on centennial time scales, similar to the relation observed in the record from a southern Oman stalagmite (*5*). The correlation coefficient for the full record is $r = 0.30$, which indicates that some of the variability in the AM can be attributed to solar changes. The main discrepancy between the two records comes at decadal time scales, plausibly reflecting fine-scale errors in chronolo-

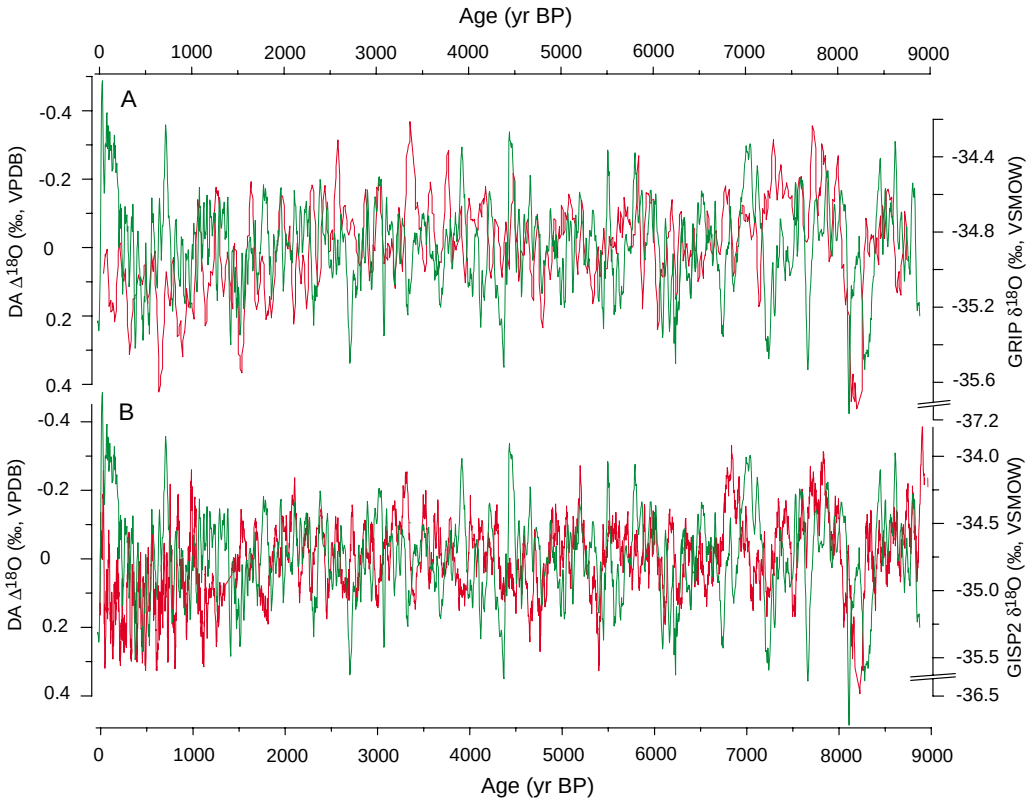

Fig. 3. Comparison of the smoothed (5-point running average) detrended DA $\Delta^{18}O$ record (green) with the smoothed 20-year averaged GRIP $\delta^{18}O$ record (5-point running average, red) (*11*) (**A**) and the GISP2 $\delta^{18}O$ record (20-point running average, red) (*12*) (**B**) over the past 9 ky. The broad correlations between DA and Greenland records are apparent at the multicentennial scale.

gy or, alternately, indicating that at these frequencies other factors may be more important in controlling AM variability, such as changes in atmospheric and oceanic circulation.

Power spectral analysis of the tuned DA $\delta^{18}O$ record shows statistically significant centennial periodicities centered on 558, 206, and 159 years (fig. S1A). These periodicities are close to significant periods of the $\Delta^{14}C$ record (512, 206, and 148 years) (*27*) and to previously reported findings from spectral analysis of another Chinese speleothem (*10*). Cross-spectral analysis of the DA record and the ^{14}C record further shows some common periodicities (232, 129, 116, 104, 89, 57, and 54 years) (fig. S1B). Our data, together with the other Chinese work (*10*) and two Oman stalagmite $\delta^{18}O$ records (*4*, *5*), support the idea that solar changes are partly responsible for changes in Holocene AM intensity (*28*).

We have previously demonstrated a close correlation between last glacial period AM variability and the temperature change over Greenland on millennial time scales (*9*, *14*). The present high-resolution DA $\delta^{18}O$ record enables a more precise correlation between the AM and Greenland climate on centennial time scales and under interglacial conditions. The smoothed, detrended DA $\Delta^{18}O$ record shows a broad similarity to the $\delta^{18}O$ records of Greenland ice—Greenland Ice Core Project (GRIP) (*11*) and Greenland Ice Sheet Project 2 (GISP2) (*12*)—in terms of frequent decadal-scale and centennial-scale fluctuations (Fig. 3). Similar to Greenland ice core records, the centennial- and multidecadal-scale AM variations during the Holocene are considerable (~0.2 to 0.7 ‰ in $\delta^{18}O$) but not as large as glacial millennial-scale variability (~1 to 2 ‰ in $\delta^{18}O$) (*9*). Because of fine-scale uncertainties in dating of records from both sites, it is not possible to determine whether decadal-scale variations correlate. However, the general correlations between DA and Greenland records are apparent on the multicentennial scale (Fig. 3). This broad correlation is also noticeable between DA and the new $\delta^{18}O$ record of Greenland ice [NGRIP (*13*)], which also has a long-term trend similar to DA between 0 and 3.8 ky B.P. (fig. S2). Over this time interval, the Pearson correlation coefficient of the records reaches its highest value of 0.57 when setting a 150-year-phase lead of the tuned DA $\delta^{18}O$ record over the NGRIP $\delta^{18}O$ time series (fig. S2). A lead of this magnitude in this time interval would be larger than the combined uncertainty in the DA ^{230}Th dating and the Greenland layer-counting chronology, but not by a large amount, because both records have errors of up to several decades. If the lead is real, given that we can attribute at least some of the variability in the AM to solar changes, it is plausible that the AM responds almost immediately to solar changes by rapid atmospheric response to solar forcing. Because Greenland's climate is closely tied to the rate of production of North Atlantic Deep Water, it is plausible that Greenland temperature lags solar forcing because of the time constants involved in changing ocean circulation. Alternatively, it is plausible that the apparent lead is not a "true" lead and that the high Pearson correlation coefficient is simply, by chance, higher with a 150-year offset. We note that the DA record has significant power at both 159-year and 206-year periods (fig. S1). Thus, the lead could plausibly represent an offset of one period at one of these frequencies.

In summary, the broad decline in AM intensity through the latter part of the Holocene correlates well with other northern low-latitude records and results directly from the orbitally induced lowering of summer insolation affecting ITCZ position and low-latitude precipitation patterns. The centennial- and multidecadal-scale events that characterize the AM record throughout can, in part, be ascribed to responses to changes in solar output. There are similarities and correlations between the Holocene AM and the North Atlantic climate, including both the ice-rafted debris record and the Greenland ice core records. Some of these correlations result from solar forcing affecting climate in both regions. It is also possible, with the 8200-year event as the main example, that oceanic circulation changes in the North Atlantic triggered changes in the AM. Thus, changes in the Holocene AM result from a number of factors, including orbitally induced insolation changes, changes in solar output, and changes in oceanic and atmospheric circulation.

References and Notes

1. G. H. Denton, W. Karlen, *Quat. Res.* **3**, 155 (1973).
2. G. Bond *et al.*, *Science* **294**, 2130 (2001).
3. F. S. Hu *et al.*, *Science* **301**, 1890 (2003).

4. U. Neff *et al.*, *Nature* **411**, 290 (2001).
5. D. Fleitmann *et al.*, *Science* **300**, 1737 (2003).
6. R. Agnihotri, K. Dutta, R. Bhushan, B. L. K. Somayajulu, *Earth Planet. Sci. Lett.* **198**, 521 (2002).
7. Z. S. An, *Quat. Sci. Rev.* **19**, 171 (2000).
8. S. C. Porter, Z. S. An, *Nature* **375**, 305 (1995).
9. Y. J. Wang *et al.*, *Science* **294**, 2345 (2001).
10. C. A. Dykoski *et al.*, *Earth Planet. Sci. Lett.*, **233**, 71 (2005).
11. W. Dansgaard *et al.*, *Nature* **364**, 218 (1993).
12. P. M. Grootes, M. Stuiver, J. W. C. White, S. J. Johnsen, J. Jouzel, *Nature* **366**, 552 (1993).
13. North Greenland Ice Core Project Members, *Nature* **431**, 147 (2004).
14. D. Yuan *et al.*, *Science* **304**, 575 (2004).
15. M. Stuiver *et al.*, *Radiocarbon* **40**, 1041 (1998).
16. K. R. Johnson, B. L. Ingram, *Earth Planet. Sci. Lett.* **220**, 365 (2004).
17. G. Haug, K. A. Hughen, D. M. Sigman, L. C. Peterson, U. Röhl, *Science* **293**, 1304 (2001).
18. X. Wang *et al.*, *Nature* **432**, 740 (2004).
19. A. K. Gupta, D. M. Anderson, J. T. Overpeck, *Nature* **421**, 354 (2003).
20. J. U. L. Baldini, F. McDermott, I. J. Fairchild, *Science* **296**, 2203 (2002).
21. D. R. Rousseau, R. Precce, N. Limondin, *Geology* **26**, 651 (1998).
22. D. C. Barber *et al.*, *Nature* **400**, 344 (1999).
23. W. Wu, T. Liu, *Quat. Int.* **117**, 153 (2004).
24. Y. T. Hong *et al.*, *Earth Planet. Sci. Lett.* **211**, 371 (2003).
25. B. Peter, *Science* **292**, 667 (2001).
26. Eighty-two time-points were selected using a criterion of $\geq\pm 10$ ‰ fluctuation in atmospheric $\Delta^{14}C$ for tuning. The tuned DA time scale is within the ^{230}Th dating error. The tuned age-depth relation remains smooth and is essentially the same as the ^{230}Th dated age-depth relation (Fig. 1B).
27. M. Stuiver, T. Braziunas, *Holocene* **3**, 289 (1993).
28. D. T. Shindell, G. A. Schmidt, M. E. Mann, D. Rind, A. Waple, *Science* **294**, 2149 (2001).
29. Supported by National Science Foundation of China grants 40225007 and 40328005, FANEDD 200227, National Basic Research Program of China 2004CB720204, U.S. NSF Grants 0214041, 0116395, and 023239, and Gary Comer Science and Education Foundation Grant CC8. The Minnesota authors thank G. Comer and W. S. Broecker for their generous support.

Supporting Online Material
www.sciencemag.org/cgi/content/full/308/5723/854/DC1
Figs. S1 and S2
Tables S1 and S2
References

12 October 2004; accepted 3 March 2005
10.1126/science.1106296

Computational Thermostabilization of an Enzyme

Aaron Korkegian,[1,2] Margaret E. Black,[4] David Baker,[3] Barry L. Stoddard[1]*

Thermostabilizing an enzyme while maintaining its activity for industrial or biomedical applications can be difficult with traditional selection methods. We describe a rapid computational approach that identified three mutations within a model enzyme that produced a 10°C increase in apparent melting temperature T_m and a 30-fold increase in half-life at 50°C, with no reduction in catalytic efficiency. The effects of the mutations were synergistic, giving an increase in excess of the sum of their individual effects. The redesigned enzyme induced an increased, temperature-dependent bacterial growth rate under conditions that required its activity, thereby coupling molecular and metabolic engineering.

Enzymes are the most efficient catalysts of chemical reactions known, enhancing reaction rates by as much as 23 orders of magnitude (*1*, *2*). However, there has been little evolutionary pressure for them to become more thermostable than is required by their native environment. Many studies indicate that enzymes (like most proteins) exhibit closely balanced free energy profiles for folding and unfolding, thereby allowing functionally important dynamic motions and appropriate degradation in vivo (*3*). However, in a laboratory or industrial setting, this lack of thermostability can lead to undesirable loss of activity (*4*).

The physical principles of protein folding that result in a balance of stability and flexibility, while maintaining function, are not perfectly understood and have been difficult to exploit for the development of thermostabilized enzymes (*4*). For hyperthermophiles, selective pressures have generated proteins with denaturation temperatures upwards of 110°C (*5*). Their proteins exhibit topologies and stabilizing interactions similar to those from mesophilic and thermophilic organisms (*6*, *7*), leading to diverse hypotheses regarding their relative behaviors (*8*). However, a key mechanism for thermostabilization appears to be the optimization of interactions between amino acids within a protein's core (*5*), complementing computational design methods that optimize a sequence for a given fold (*9*–*13*).

The thermostabilization of an enzyme presents additional challenges for computational protein design methods, because the active-site substrate geometry and the molecular dynamic behavior during an enzymatic reaction often appear fine-tuned for maximum catalytic efficiency (*2*, *3*). Therefore, the design method must be capable of predicting thermostabilizing mutations within a given fold while minimizing any shift in the backbone that might structurally disrupt the active-site structure or quench its flexibility.

In the past several years, methods for computational protein structure prediction and design have improved substantially (*10*, *11*, *14*). Recently, computational design has been used successfully in thermostabilizing noncatalytic proteins (*15*–*18*), redesigning binding pockets (*19*–*23*), creating a protein fold (*24*), and designing catalytic activity into a bacterial receptor (*25*). We use the program RosettaDesign (*26*), which uses an energy function for evaluating the fitness of a particular sequence for a given fold and a Metropolis Monte Carlo search algorithm for sampling sequence space. The program requires a backbone structure as input and generates sequences that have the lowest energy for that fold.

We picked the homodimeric hydrolase enzyme yeast cytosine deaminase (yCD), which converts cytosine to uracil, as a target for computational thermostabilization. yCD was chosen because its high-resolution crystal structure is available (*27*), its catalytic mechanism is well characterized (*27*), it is thermolabile (*28*, *29*), and it has potential use in antitumor suicide gene applications (*27*, *29*–*31*). As do many commercially useful enzymes, yCD displays irreversible unfolding behavior at high temperatures (presumably because of aggregation) rather than the more simple, fully reversible behavior common among model systems for the study of protein folding. The problems inherent in engineering such catalysts have been recently reviewed (*4*). We used computational redesign to predict a series of point mutations in the enzyme core that might lead to thermostabilization of the enzyme without losing catalytic efficiency. We then prepared a series of designed enzyme variants and determined their folded thermostability, catalytic behavior, ability to complement metabolic cytosine deaminase activity, and three-dimensional crystal structures.

Our general computational strategy was largely unchanged from that described by Kuhlman and Baker (*26*, *32*). An energy function evaluated target sequences threaded onto a template backbone (*12*, *13*, *26*, *33*). Sequence space was searched with an iterative Metropolis Monte Carlo procedure, starting with a random sequence, replacing a single amino acid rotamer with a rotamer from the Dunbrack backbone-dependent rotamer library (*34*), and reevaluating the energy. Sequences with lower energy were automatically adopted, whereas

[1]Division of Basic Sciences, Fred Hutchinson Cancer Research Center (FHCRC), 1100 Fairview Avenue North, Seattle, WA 98109, USA. [2]Graduate Program in Molecular and Cellular Biology, [3]Department of Biochemistry and Howard Hughes Medical Institute, University of Washington, Seattle, WA 98195, USA. [4]Department of Pharmaceutical Sciences, College of Pharmacy, Washington State University, Pullman, WA 99164–6534, USA.

*To whom correspondence should be addressed. E-mail: bstoddar@fhcrc.org